Vacuum 233 (2025) 113944

Contents lists available at ScienceDirect

Vacuum

journal homepage: www.elsevier.com/locate/vacuum

Determination of the actual valence band of a topological insulator Bi_2Se_3

Yuki Higuchi [a], Ryota Itaya [a], Harutaka Saito [b], Yuichiro Toichi [a], Takahiro Kobayashi [c], Mito Tomita [a], Shigemi Terakawa [a,d], Katsuhiro Suzuki [e], Kenta Kuroda [f,g], Takao Kotani [h,i], Fumihiko Matsui [j], Shigemasa Suga [k], Hitoshi Sato [l], Kazunori Sato [b,i,m], Kazuyuki Sakamoto [a,i,m,*]

[a] Department of Applied Physics, Graduate School of Engineering, Osaka University, Osaka 565-0871, Japan
[b] Division of Materials and Manufacturing Science, Graduate School of Engineering, Osaka University, Osaka 565-0871, Japan
[c] Department of Material and Life Science, Graduate School of Engineering, Osaka University, Osaka 565-0871, Japan
[d] Center for Future Innovation, Graduate School of Engineering, Osaka University, Osaka 565-0871, Japan
[e] Department of Mechanical Engineering, National Institute of Technology, Niihama College, Ehime 792-0805, Japan
[f] Department of Physical Science, Graduate School of Advanced Science and Engineering, Hiroshima University, Hiroshima 739-8526, Japan
[g] International Institute for Sustainability with Knotted Chiral Meta Matter (SKCM^2), Hiroshima University, Hiroshima 739-8526, Japan
[h] Advanced Mechanical and Electronic System Research Center, Department of Engineering, Tottori University, Tottori 680-8552, Japan
[i] Center for Spintronics Research Network, Graduate School of Engineering Science, Osaka University, Osaka 560-8531, Japan
[j] UVSOR Synchrotron Facility, Institute for Molecular Science, Aichi 444-8585, Japan
[k] SANKEN, Osaka University, Osaka 567-0047, Japan
[l] Hiroshima Research Institute for Synchrotron Radiation Science, Hiroshima University, Higashi-Hiroshima 739-0046, Japan
[m] Spintronics Research Network Division Institute for Open and Transdisciplinary Research Initiatives, Osaka University, Osaka 565-0871, Japan

ARTICLE INFO

MSC:
00-01
99-00

Keywords:
Topological insulator
Bi_2Se_3
Direct band gap semiconductor
ARPES
DFT calculation
Quasi-particle self-consistent *GW*

ABSTRACT

A proper understanding of the electronic structure of topological insulators in terms of bulk states as well as surface spin polarized states is essential for the development of spintronic devices. In this work, we investigated the electronic structure of Bi_2Se_3, a typical n-type topological insulator. Experimentally, we measured the band dispersions along $\bar{\Gamma}$-$\bar{M}$ and the constant energy contours in the entire three-dimensional Brillouin zone, and confirmed that the valence band maximum is located at the Γ point with a binding energy 65 ± 15 meV higher than that of the Dirac point. The theoretical calculations performed by a quasi-particle self-consistent *GW* method show good agreement with the experimental results on the bulk band structure. The present results indicate that Bi_2Se_3 is a suitable candidate for next-generation spintronic devices.

1. Introduction

Three-dimensional (3D) topological insulators (TIs) are unique materials with topologically protected metallic surface states with Dirac-cone (DC) shape that span the bulk band gap and are characterized by linear dispersion and helical spin texture with spin locked perpendicular to momentum. The binding energy (E_B) of the Dirac point (DP) with respect to the Fermi level (E_F) can be controlled by charge doping [1–3], allowing a transition between p-type and n-type TI, where the DP is located at a E_B lower and higher than that of E_F, respectively. These properties make the TIs promising candidates for next-generation spintronics devices such as topological p–n junction [4] and charge-to-spin conversion device via the Edelstein effect [5].

Bi_2Se_3 is a typical n-type TI [2,6,7] due to thermodynamically stable Se defects and Bi substitution of Se formed during the crystal growth [8–11]. Its structure is formed by a rhombohedral unit cell (Fig. 1(a)) composed of Se_1-Bi-Se_2-Bi-Se_1 quintuple layers (QLs) stacked by weak van der Waals interaction along the [111] direction (Fig. 1(b)). Single crystals of Bi_2Se_3 are easily cleaved in the (111) plane and the Se_1 plane appears at the surface [12]. To exploit the many fascinating properties associated with the Bi_2Se_3 topological surface states, only the DC should cross E_F and the bulk band gap must be fully open. It is therefore significant to determine the bulk band structure as well as the DC surface states.

While previous studies agreed that the conduction band minimum (CBM) is located at the Γ point of the 3D Brillouin zone (BZ) (Fig. 1(c)), there is still a debate about the position of the valence band maximum (VBM); it is unclear whether the bulk bands have an indirect or direct band gap. Previous density functional theory (DFT) calculations reported that the VBM of Bi_2Se_3 is located on the Z-F line of the 3D

* Corresponding author.
E-mail addresses: yhiguchi@ap.eng.osaka-u.ac.jp (Y. Higuchi), kazuyuki_sakamoto@ap.eng.osaka-u.ac.jp (K. Sakamoto).

https://doi.org/10.1016/j.vacuum.2024.113944
Received 30 September 2024; Received in revised form 4 December 2024; Accepted 10 December 2024
Available online 16 December 2024

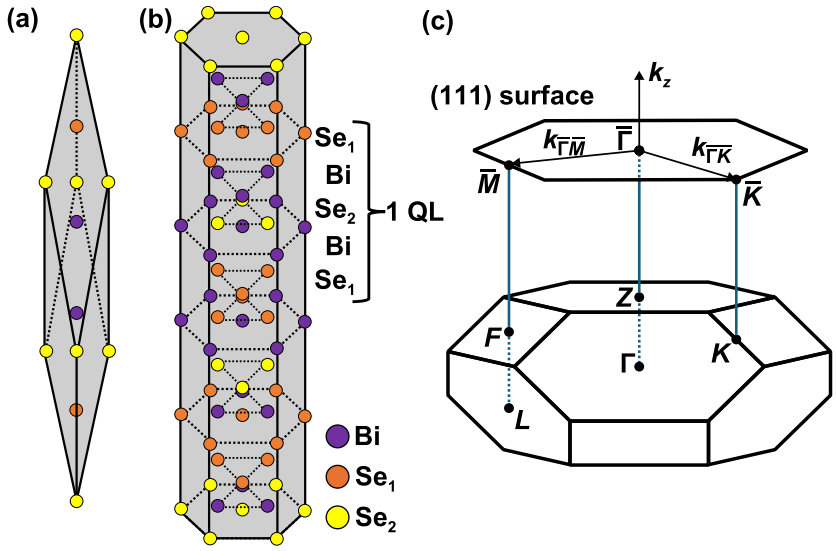

Fig. 1. (a) The rhombohedral primitive unit cell of Bi_2Se_3. (b) The layered structure of Bi_2Se_3 with the Se_1-Bi-Se_2-Bi-Se_1 quintuple layer (QL) stacked along the [111] direction. (c) The 3D Brillouin zone and the 2D Brillouin zone projected onto the (111) plane.

BZ, which corresponds to the $\bar{\Gamma}$-$\bar{M}$ line of the two-dimensional (2D) BZ, and at an E_B lower than or equal to that of the DP [6,7,13–15]. The bulk DFT calculations were performed with the full-potential linearized augmented plane-wave method (FLAPW) within the generalized gradient approximation (GGA) [16] or the plane-wave pseudopotential method (PWP) within the local density approximation (LDA) [17]. This theoretically obtained VBM location was also supported experimentally by a scanning tunneling microscope (STM) measurement [14]. On the other hand, bulk calculations performed by linearized muffin-tin orbital method (LMTO) within LDA [18] and *GW* methods show that the VBM is located at the Γ point [19–21], indicating the bulk band to have a direct band gap. The direct band gap nature of Bi_2Se_3 was experimentally supported using photoluminescence, infrared transmission and galvanomagnetic property measurements [22–25]. An angle-resolved photoelectron spectroscopy (ARPES) study [19] performed using a highly electron doped Bi_2Se_3 also suggested that the VBM is located at the $\bar{\Gamma}$ point and at a E_B higher than that of the DP.

In this study, we experimentally investigate the band structure of Bi_2Se_3 not only along the high symmetry lines but also in the whole 3D BZ with the complementary use of a conventional ARPES setup and a photoelectron momentum microscope. The VBM is found to be located at the $\bar{\Gamma}$ point and at a E_B higher than that of the DP. These results are well reproduced by our theoretical calculations obtained by a quasi-particle self-consistent *GW* (QSGW) calculation [26,27].

2. Materials and methods

The ARPES measurements were performed using two different types of analyzers. To observe the band dispersions along $k_{//}$, a high-resolution hemispherical electron energy analyzer (SES2002, SCIENTA) with an overall energy resolution better than 60 meV was used at the beamline BL-7 of the Hiroshima Synchrotron Radiation Center (HiSOR), Japan. To observe the constant energy contours at different E_B throughout the entire 3D BZ, we used a photoelectron momentum microscope type analyzer (KREIOS 150MM, SPECS) at the BL6U [28] of the UVSOR synchrotron facility, Institute for Molecular Science, Japan. The overall energy resolution and momentum resolution of this system were better than 20 meV and 0.01 $Å^{-1}$, respectively. The k_z value was obtained using Eq. (1) assuming a free-electron final state:

$$\hbar k_z = \sqrt{2m_e(E_{kin}\cos^2\theta + V_0)}. \quad (1)$$

Here, E_{kin} and θ are the kinetic energy and emission angle of photoelectrons, and V_0 is the inner potential. In this study, we used V_0 = 11.8 eV according to the value reported in the former studies of Bi_2Se_3 [2,6].

High-quality single-crystalline Bi_2Se_3 samples, grown by the Bridgman method, were cleaved *in situ* at room temperature using the Scotch tape method at UVSOR and using the post-knocking method at HiSOR to obtain clean surfaces. The sizes of the samples were approximately $2.6 \times 2.1 \times 0.5$ mm^3 at HiSOR and $3.6 \times 2.6 \times 0.5$ mm^3 at UVSOR. The ARPES measurements were performed at 50 K at UVSOR and at 10 K at HiSOR. The base pressures of the ARPES measurement chambers were $< 2.0 \times 10^{-8}$ Pa at UVSOR and $< 2.1 \times 10^{-8}$ Pa at HiSOR. Samples were checked for in-plane orientation by Laue diffraction before being placed in the vacuum chamber.

Theoretical calculations were performed using the QSGW method (QSGW-60 [29]) and the LDA method implemented in the ecalj package [26,27,30]. The QSGW method incorporating many-body effects is an excellent method to evaluate the band gaps [29]. The experimentally determined cell parameters [31,32] of the rhombohedral primitive cell, which show good agreement with the computational ones obtained from the relaxation procedure within the GGA calculations [19], were used in the calculations. The spin–orbit coupling (SOC) effect was included perturbatively, and a k-point mesh of 8 × 8 × 8 was adopted for the electronic band structure calculations.

3. Results and discussion

In order to obtain information of the position of the VBM relative to the DP, we have measured the band dispersions of Bi_2Se_3 along $\bar{\Gamma}$-$\bar{M}$ with photon energies ($h\nu$) from 35 to 89 eV in 2 eV step, a $h\nu$ range that has not been used in the previous study [19]. This $h\nu$ range corresponds to a k_z range from 3.33 to 5.03 $Å^{-1}$ under the direct emission condition at E_F. In Figs. 2(a-d) are the band dispersions along $\bar{\Gamma}$-$\bar{M}$ at four different $h\nu$. The DC is clearly seen and the DP is found at E_B= 0.3 eV. By considering the difference in E_B of the CBM and DP reported in former studies [2,33–35], the results in Figs. 2(a-d) indicate that the conduction band (CB) of the present sample is crossing the E_F. The valence band (VB) is clearly observed around the $\bar{\Gamma}$ point at $h\nu$ = 57 eV and together with an upward-convex-shaped band with a local maximum at around 0.45 $Å^{-1}$ at $h\nu$ = 47 and 77 eV. Taking into account that Bi_2Se_3 has been reported to have its VBM at around $k_{//} = 0.3$ $Å^{-1}$ along $\bar{\Gamma}$-$\bar{M}$ [14], we investigated the k_z-dependent

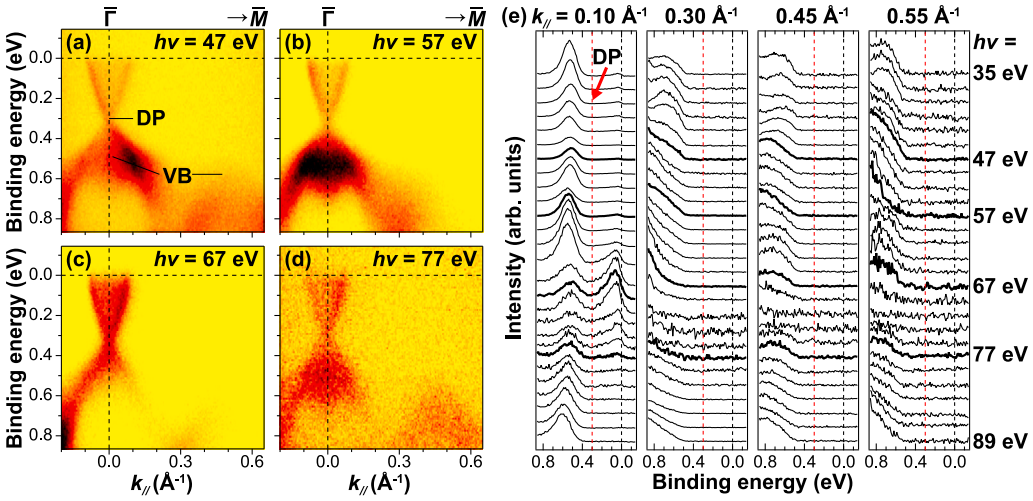

Fig. 2. Band dispersions along $\bar{\Gamma}$-$\bar{M}$ of Bi_2Se_3(111) measured at $h\nu$ = (a) 47 eV, (b) 57 eV, (c) 67 eV and (d) 77 eV. (e) $h\nu$ dependent-EDCs at $k_{//}$ = 0.10, 0.30, 0.45 and 0.55 Å^{-1} along $\bar{\Gamma}$-$\bar{M}$ measured with $h\nu$ from 35 to 89 eV in 2 eV steps. The EDCs in $\Delta k_{//}$ = 0.05 Å^{-1} were averaged in (e). The EDC at $h\nu$ = 53 eV was excluded due to the strong contribution from the Se 3d peak excited by the second-order light. The red dotted lines denote the E_B of the DP. The measurements were performed at 10 K.

energy distribution curves (ECDs) at $k_{//}$ = 0.10, 0.30, 0.45, 0.55 Å^{-1} to determine the VBM. The red dotted lines in Fig. 2(e) indicate the E_B of the DP. At any points of $k_{//}$, the bulk VB is located at E_B higher than 0.4 eV, which indicates that the VB along $\bar{\Gamma}$-$\bar{M}$ is always located at E_B higher than that of the DP. Furthermore, as $k_{//}$ value moves from 0.10 Å^{-1} to 0.55 Å^{-1}, the VB goes downward toward the high E_B side. These results indicate that the VBM is located at the $\bar{\Gamma}$ point. Since the VBM can exist at $k_{//}$ other than on the $\bar{\Gamma}$-$\bar{M}$ line, we measured the constant energy contours of Bi_2Se_3 from $h\nu$ = 60 eV to 120 eV in 4 eV step. This $h\nu$ range covers more than two 3D BZs in the Γ-Z direction (Γ-Z = 0.33 Å^{-1}). In Fig. 3 are the constant energy contours at E_B = 0.1, 0.3, 0.5 and 0.7 eV measured using $h\nu$ = 72, 80, 92, 100, 116, and 120 eV, which correspond to k_z = 4.56, 4.78, 5.10, 5.30, 5.69, and 5.78 Å^{-1} under the direct emission condition at E_F. The dashed lines represent the 2D BZ of Bi_2Se_3, and its symmetry points $\bar{\Gamma}$, $\bar{M}$, and $\bar{K}$ are indicated in the top-left image of Fig. 3(a). (The fullset of the constant energy contours are shown in Figs. S2 and S3 of the supplementary material [36].) At E_B = 0.10 eV (Fig. 3(a)), all contours consist of circles centered at $\bar{\Gamma}$. As the E_B increases, the radii of circles become smaller, reach a minimum value at around E_B= 0.3 eV (Fig. 3(b)) and become larger again at higher E_B (Fig. 3(c)). The minimum value of the radius indicates the DP to be located at E_B= 0.3 eV, which agrees well with the results in Fig. 2. Since the CBM is reported to be at a E_B 0.2 eV lower than that of the DP [2,33–35], the CBM should be located at E_B = 0.1 eV. The radius at E_B = 0.1 eV is changing depending on the $h\nu$, and it indicates the contribution of not only the DC and but also the bulk CB. (Note that the change in radius is visible due to the finite energy window caused by the energy resolution of the system.) Blurred features appear along the $\bar{\Gamma}$-$\bar{M}$ direction at E_B = 0.5 eV, when using $h\nu$ = 92 eV (Fig. 3(c)), and they become clearer at E_B = 0.7 eV, when using $h\nu$ =80, 92, and 100 eV (Fig. 3(d)). The features exhibit strong $h\nu$ dependence and thus are attributed to the bulk VB. The contours at E_B = 0.7 eV at $h\nu$ = 80 and 116 eV exhibit six-fold rotational symmetry. On the other hand, the contours at $h\nu$ = 72, 92, 100, and 120 eV have three-fold rotational symmetry with a three-bladed propeller-like shape whose direction is reversed between $h\nu$ =72 and 120 eV and $h\nu$ = 92 and 100 eV. The six-fold patterns are attributed to the bands on the $k_{//}$ plane either centered at the Γ point or the Z point in the 3D BZ, and the three-fold ones are to the bands on the $k_{//}$ planes between those two planes.

To investigate the origin of the contradictory location of the VBM in former theoretical studies, we have performed calculations using two different methods, QSGW and LDA. In Fig. 4 is the bulk band structure along the high-symmetry lines of the 3D BZ calculated by QSGW and LDA, with and without including the SOC. As shown in Figs. 4(a,b), the uppermost VB exhibits convex shapes around the Γ point and on the Z-F line, and the E_B of the top of the convex on the Z-F line is higher than that at the Γ point in the two calculations performed without SOC. Note that in calculations without SOC, the band gap calculated by QSGW is usually larger than that obtained by LDA owing to the way of handling many-body effects [29]. When the SOC is perturbatively included, the convex-shaped VB at Γ undergoes the band inversion with the CB, and the band structures obtained by LDA and QSGW show a significant difference. In the LDA calculation, the significant overlap of the VB and CB resulting from the small band gap before including SOC makes the band inversion area large and changes the convex-shaped VB at Γ to a camelback shape [21]. Consequently, the top of the VB around the Γ has almost the same E_B as that of the convex shape on the Z-F line (Fig. 4(c)). In the QSGW calculation, the small overlap of the VB and CB due to the large band gap before including SOC produces only a small inversion area that is not sufficient to change the shape of the VB at the Γ point. The convex shape at Γ is preserved and its E_B remains lower than that of the top along the Z-F line (Fig. 4(d)). Since the Bi $6p_z$ and Se_1 $4p_z$ states are involved in the band inversion [13], we discuss the contribution of the Bi p_z and Se_1 p_z orbitals to the bulk VB and CB around the Γ point to get insight into the SOC-driven band inversion. The color scale I in Fig. 4 defined by Eq. (2) indicates the contribution of the two orbitals.

$$I = \frac{-p_z^2(\mathrm{Se}_1) + p_z^2(\mathrm{Bi})}{p_z^2(\mathrm{Se}_1) + p_z^2(\mathrm{Bi})}. \quad (2)$$

Here, p_z(Bi) and p_z(Se_1) are the projections of the Bi p_z and Se_1 p_z orbital bases onto the LDA or QSGW wave functions. In the calculations performed without SOC, each p_z state is completely separated, i.e. the CB and VB are composed of only Bi p_z (blue) and Se_1 p_z (red), respectively. In the case of including SOC, both calculations exhibit the band inversion at the Γ point, i.e. the CB and VB consist of Se_1 p_z (red) and Bi p_z (blue), respectively. This means that, although the VB shape at Γ does not change significantly, band inversion occurs in the QSGW calculation as well.

The 3D bulk band dispersion is projected onto the (111) plane of Bi_2Se_3 in Fig. 5 to compare the theoretically obtained bands with those obtained experimentally. The band dispersion by LDA including SOC indicates that the VBM is in the middle of the $\bar{\Gamma}$-$\bar{M}$ line (Fig. 5(a)). On the other hand, the QSGW including SOC shows that the VBM is located at $\bar{\Gamma}$ and reproduces well the VBM obtained experimentally (Fig. 5(b)). Moreover, not only the location of the VBM but also the dispersion

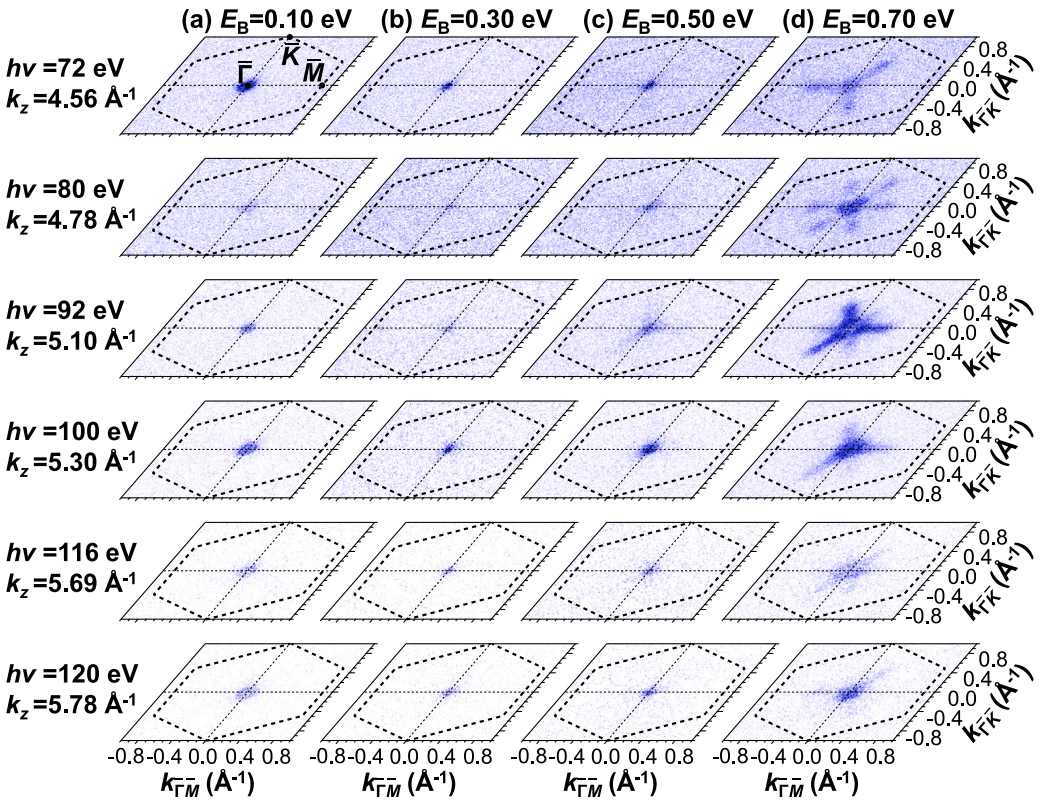

Fig. 3. Constant energy contours (-1.0 Å^{-1} $< k_{//} <$ 1.0 Å^{-1}) of Bi_2Se_3(111) at E_B of (a) 0.10 eV, (b) 0.30 eV, (c) 0.50 eV and (d) 0.70 eV measured with $h\nu$ = 72, 80, 92, 100, 116, 120 eV at 50 K. The k_z values on the left are calculated under the direct emission condition at E_F. The dashed line on the each image represents the 2D BZ of Bi_2Se_3.

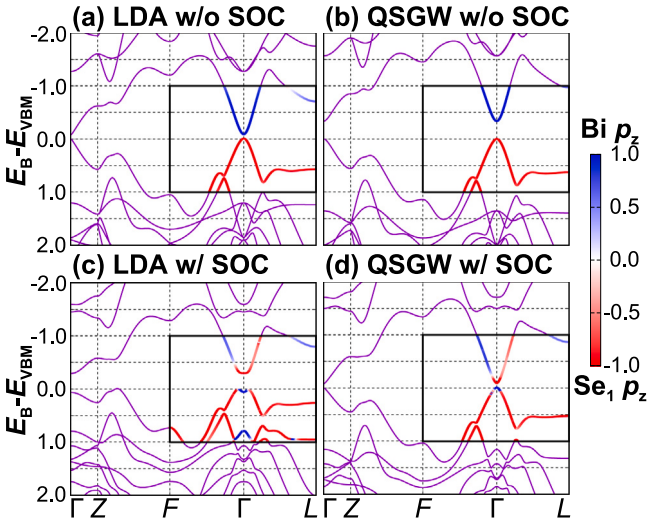

Fig. 4. Bulk band dispersions of Bi_2Se_3 obtained by (a) LDA and (b) QSGW without (w/o) SOC, and those obtained by (c) LDA and (d) QSGW with (w/) SOC. The color of the band along F-Γ-L represents the contribution of the Bi p_z and Se_1 p_z orbitals as indicated in the scale bar.

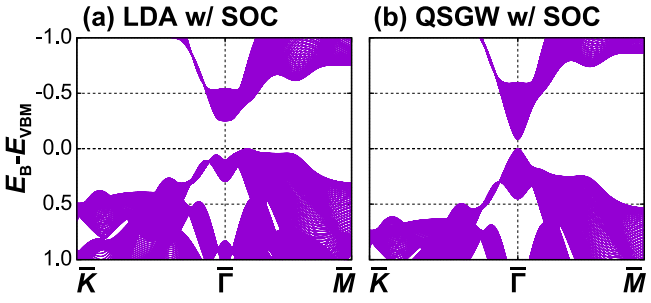

Fig. 5. Bulk band dispersions of Bi_2Se_3 projected on the 2D BZ along $\bar{M}$-$\bar{\Gamma}$-$\bar{K}$ using (a) LDA and (b) QSGW including SOC.

feature from $\bar{\Gamma}$ to $\bar{M}$ obtained with QSGW shows good agreement with the experimentally obtained dispersion, including the nearly flat dispersion around the midpoint of $\bar{\Gamma}$-$\bar{M}$ and the downward dispersion toward $\bar{M}$.

The constant energy contours of the (111) plane of Bi_2Se_3 obtained by QSGW including SOC for several k_z are shown in Fig. 6 to compare the experimentally obtained constant energy contours with the theoretical ones. (Those calculated using LDA including SOC are shown in Fig. S3 of the supplementary material [36].) At $E_B - E_{VBM}$ = 0.05 eV (Fig. 6(a)), a contour centered at $\bar{\Gamma}$ is found only at k_z = 0.00 Å^{-1}, indicating that the VBM is located at the Γ point of the 3D BZ. This result is in consistent with the experimentally obtained k value of the VBM. As $E_B - E_{VBM}$ becomes higher at k_z = 0 Å^{-1}, the contour centered at $\bar{\Gamma}$ becomes larger. At $E_B - E_{VBM}$ = 0.25, 0.35 eV, the contours at k_z = 0 Å^{-1} (Γ) and 0.33 Å^{-1} (Z) have shapes with six-fold rotational symmetry, which agree with those obtained experimentally at the $k_{//}$ planes centered at the Γ point or the Z point in Figs. 3(c,d). The contours at k_z = 0.08, 0.16, 0.25 Å^{-1} have three-fold rotational symmetry, which are also consistent with the experimental results.

Although the calculated bulk band dispersions and constant energy contours reproduce well the ARPES results, the band gap obtained by QSGW with SOC at $\bar{\Gamma}$, 0.09 eV, is much smaller than the experimental value that is larger than 0.2 eV. The calculated band gap will be further improved by treating the SOC effect in a self-consistent way rather than in a perturbative way, but it is beyond the scope of this work. Furthermore, the present result does not agree with the former STM study [14], which suggested that the VBM is located in the middle

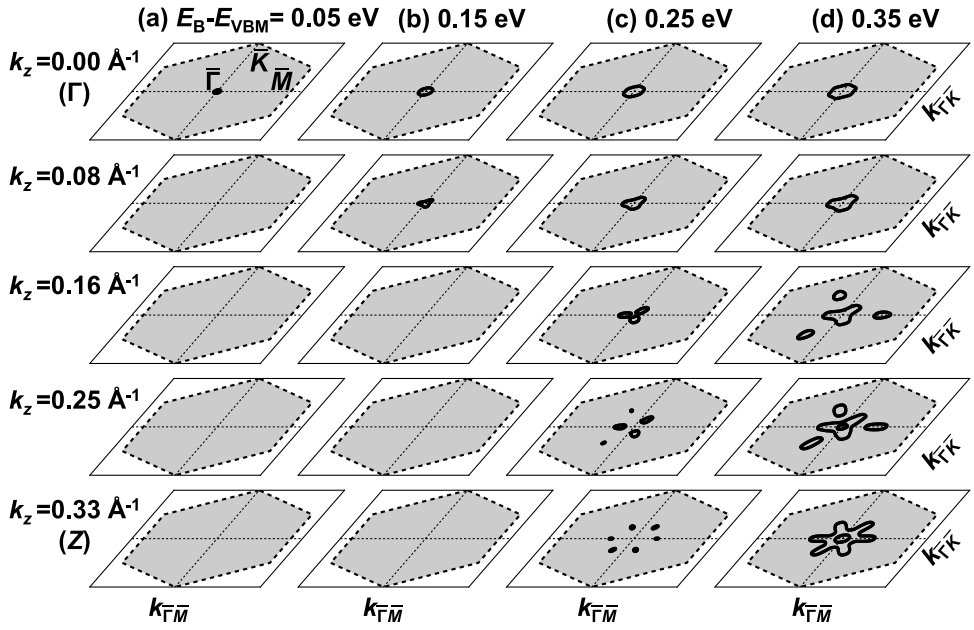

Fig. 6. Constant energy contours of Bi_2Se_3(111) calculated using QSGW with SOC at $E_B - E_{VBM}$ = (a) 0.05 eV, (b) 0.15 eV, (c) 0.25 eV and (d) 0.35 eV. The k_z values on the left indicate the positions in the 3D BZ; k_z = 0.00 Å^{-1} is the Γ point and k_z = 0.33 Å^{-1} is the Z point. The hexagon colored in gray on each image represents the 2D BZ of Bi_2Se_3. A small part of the contours is missing at $E_B - E_{VBM}$ = 0.25 eV and k_z = 0.25 Å^{-1} because the number of the k points for the band structure calculation was insufficient to resolve it.

of the $\bar{\Gamma}$-$\bar{M}$ line with its E_B almost the same as that of the DP. In this STM study, the location of the VBM was discussed based on the fast Fourier transformation (FFT) of the dI/dV images, which show the possibility of electron scattering between the surface DC state and bulk electronic states. However, since the scattering vector obtained from the FFT patterns shows almost no E_B dependence, the interference pattern observed in FFT might not be a result from the surface-bulk scattering but rather a phenomenon related to surface electrons trapped in non-dispersive impurity levels.

4. Conclusions

In conclusion, we have investigated the electronic structure of Bi_2Se_3 using both experimental and computational methods. By measuring the band structure along the high symmetry $\bar{\Gamma}$-$\bar{M}$ line and the constant energy contours at different E_B using a wide range of $h\nu$, we found that the bulk VBM is located at the Γ point of the 3D BZ. This result indicates that the bulk electronic structure of Bi_2Se_3 has a direct band gap with the VBM at the Γ point. Regarding the computational results, the projected bulk band dispersion and constant energy contours obtained by the QSGW method well reproduce the ARPES results. Furthermore, the QSGW calculations show that the band inversion occurs at the Γ point. This shows the usefulness of high-precision calculations that include electron many-body effects for the determination of the actual electronic structure of topological insulators. Taking into account that it is possible to dope hole into the n-type Bi_2Se_3, the present results demonstrate the high prospects of this material for future spintronics applications such as topological p–n junction.

CRediT authorship contribution statement

Yuki Higuchi: Writing – original draft, Visualization, Project administration, Investigation, Data curation, Conceptualization. **Ryota Itaya:** Investigation. **Harutaka Saito:** Investigation. **Yuichiro Toichi:** Investigation. **Takahiro Kobayashi:** Investigation. **Mito Tomita:** Investigation. **Shigemi Terakawa:** Writing – review & editing, Visualization, Project administration, Data curation. **Katsuhiro Suzuki:** Investigation. **Kenta Kuroda:** Resources. **Takao Kotani:** Investigation. **Fumihiko Matsui:** Investigation. **Shigemasa Suga:** Investigation. **Hitoshi Sato:** Investigation. **Kazunori Sato:** Investigation. **Kazuyuki Sakamoto:** Writing – review & editing, Supervision, Project administration, Investigation, Funding acquisition, Conceptualization.

Declaration of competing interest

The authors declare that they have no known competing financial interests or personal relationships that could have appeared to influence the work reported in this paper.

Acknowledgments

This work was supported by the JSPS, Japan KAKENHI Grants No. JP24K23032, JP22H01957, JP22H01943, JP22AG002, JP22BU007, JP22K04909, JP20H05621, and JP20K03863, and the Spintronics Research Network of Japan. Y.H. was supported by the JST SPRING, Japan Grant No. JPMJSP2138, and the Program for Leading Graduate Schools: “Interactive Materials Science Cadet Program” of Osaka University, Japan. The experiments at HiSOR were performed under the approval of the Program Advisory Committee (Proposal No. 22BU007), and those at UVSOR were conducted by Cooperative Research (IMS program 23IMS1216).

Appendix A. Supplementary data

Supplementary material related to this article can be found online at https://doi.org/10.1016/j.vacuum.2024.113944.

Data availability

Data will be made available on request.

References

[1] C. Seibel, H. Maaß, M. Ohtaka, S. Fiedler, C. Jünger, C.-H. Min, H. Bentmann, K. Sakamoto, F. Reinert, Single Dirac cone on the Cs-covered topological insulator surface Sb_2Te_3 (0001), Phys. Rev. B 86 (2012) 161105, http://dx.doi.org/10.1103/PhysRevB.86.161105.

[2] M. Bianchi, D. Guan, S. Bao, J. Mi, B.B. Iversen, P.D. King, P. Hofmann, Coexistence of the topological state and a two-dimensional electron gas on the surface of Bi_2Se_3, Nature Commun. 1 (2010) 128, http://dx.doi.org/10.1038/ncomms1131.

[3] K. Sakamoto, H. Ishikawa, T. Wake, C. Ishimoto, J. Fujii, H. Bentmann, M. Ohtaka, K. Kuroda, N. Inoue, T. Hattori, T. Miyamachi, F. Komori, I. Yamamoto, C. Fan, P. Krüger, H. Ota, F. Matsui, F. Reinert, J. Avila, M.C. Asensio, Spatial control of charge doping in n-type topological insulators, Nano Lett. 21 (2021) 4415–4422, http://dx.doi.org/10.1021/acs.nanolett.1c01100.

[4] N.H. Tu, Y. Tanabe, Y. Satake, K.K. Huynh, K. Tanigaki, In-plane topological p-n junction in the three-dimensional topological insulator $Bi_{2-x}Sb_xTe_{3-y}Se_y$, Nature Commun. 7 (2016) 13763, http://dx.doi.org/10.1038/ncomms13763.

[5] S. Zhang, A. Fert, Conversion between spin and charge currents with topological insulators, Phys. Rev. B 94 (2016) 184423, http://dx.doi.org/10.1103/PhysRevB.94.184423.

[6] Y. Xia, D. Qian, D. Hsieh, L. Wray, A. Pal, H. Lin, A. Bansil, D. Grauer, Y.S. Hor, R.J. Cava, M.Z. Hasan, Observation of a large-gap topological-insulator class with a single Dirac cone on the surface, Nat. Phys. 5 (2009) 398–402, http://dx.doi.org/10.1038/nphys1274.

[7] D. Hsieh, Y. Xia, D. Qian, L. Wray, J.H. Dil, F. Meier, J. Osterwalder, L. Patthey, J.G. Checkelsky, N.P. Ong, A.V. Fedorov, H. Lin, A. Bansil, D. Grauer, Y.S. Hor, R.J. Cava, M.Z. Hasan, A tunable topological insulator in the spin helical Dirac transport regime, Nature 460 (2009) 1101–1105, http://dx.doi.org/10.1038/nature08234.

[8] J. Horák, Z. Stary, P. Lošťák, J. Pancíř, Anti-site defects in n-Bi_2Se_3 crystals, J. Phys. Chem. Solids 51 (1990) 1353–1360, http://dx.doi.org/10.1016/0022-3697(90)90017-A.

[9] S. Urazhdin, D. Bilc, S.H. Tessmer, S.D. Mahanti, T. Kyratsi, M.G. Kanatzidis, Scanning tunneling microscopy of defect states in the semiconductor Bi_2Se_3, Phys. Rev. B 66 (2002) 161306, http://dx.doi.org/10.1103/PhysRevB.66.161306.

[10] S.S. Lin, C.N. Liao, Effect of ball milling and post treatment on crystal defects and transport properties of $Bi_2(Se,Te)_3$ compounds, J. Appl. Phys. 110 (2011) 093707, http://dx.doi.org/10.1063/1.3658256.

[11] L. Xue, P. Zhou, C.X. Zhang, C.Y. He, G.L. Hao, L.Z. Sun, J.X. Zhong, First-principles study of native point defects in Bi_2Se_3, AIP Adv. 3 (2013) 052105, http://dx.doi.org/10.1063/1.4804439.

[12] V.V. Atuchin, V.A. Golyashov, K.A. Kokh, I.V. Korolkov, A.S. Kozhukhov, V.N. Kruchinin, S.V. Makarenko, L.D. Pokrovsky, I.P. Prosvirin, K.N. Romanyuk, O.E. Tereshchenko, Formation of inert Bi_2Se_3(0001) cleaved surface, Cryst. Growth Des. 11 (2011) 5507–5514, http://dx.doi.org/10.1021/cg201163v.

[13] H. Zhang, C.-X. Liu, X.-L. Qi, X. Dai, Z. Fang, S.-C. Zhang, Topological insulators in Bi_2Se_3, Bi_2Te_3 and Sb_2Te_3 with a single Dirac cone on the surface, Nat. Phys. 5 (2009) 438–442, http://dx.doi.org/10.1038/nphys1270.

[14] S. Kim, M. Ye, K. Kuroda, Y. Yamada, E.E. Krasovskii, E.V. Chulkov, K. Miyamoto, M. Nakatake, T. Okuda, Y. Ueda, K. Shimada, H. Namatame, M. Taniguchi, A. Kimura, Surface scattering via bulk continuum states in the 3D topological insulator Bi_2Se_3, Phys. Rev. Lett. 107 (2011) 056803, http://dx.doi.org/10.1103/PhysRevLett.107.056803.

[15] S.V. Eremeev, Y.M. Koroteev, E.V. Chulkov, Effect of the atomic composition of the surface on the electron surface states in topological insulators $A_2^VB_3^{VI}$, JETP Lett. 91 (2010) 387–391, http://dx.doi.org/10.1134/S0021364010080059.

[16] P. Larson, V.A. Greanya, W.C. Tonjes, R. Liu, S.D. Mahanti, C.G. Olson, Electronic structure of Bi_2X_3 (X=S , Se , T) compounds: Comparison of theoretical calculations with photoemission studies, Phys. Rev. B 65 (2002) 085108, http://dx.doi.org/10.1103/PhysRevB.65.085108.

[17] O.V. Yazyev, E. Kioupakis, J.E. Moore, S.G. Louie, Quasiparticle effects in the bulk and surface-state bands of Bi_2Se_3 and Bi_2Te_3 topological insulators, Phys. Rev. B 85 (2012) 161101, http://dx.doi.org/10.1103/PhysRevB.85.161101.

[18] S.K. Mishra, S. Satpathy, O. Jepsen, Electronic structure and thermoelectric properties of bismuth telluride and bismuth selenide, J. Phys.: Condens. Matter. 9 (1997) 461–470, http://dx.doi.org/10.1088/0953-8984/9/2/014.

[19] I.A. Nechaev, R.C. Hatch, M. Bianchi, D. Guan, C. Friedrich, I. Aguilera, J.L. Mi, B.B. Iversen, S. Blügel, P. Hofmann, E.V. Chulkov, Evidence for a direct band gap in the topological insulator Bi_2Se_3 from theory and experiment, Phys. Rev. B 87 (2013) 121111, http://dx.doi.org/10.1103/PhysRevB.87.121111.

[20] I. Aguilera, C. Friedrich, G. Bihlmayer, S. Blügel, *GW* study of topological insulators Bi_2Se_3, Bi_2Te_3, and Sb_2Te_3: Beyond the perturbative one-shot approach, Phys. Rev. B 88 (2013) 045206, http://dx.doi.org/10.1103/PhysRevB.88.045206.

[21] I. Aguilera, C. Friedrich, S. Blügel, Many-body corrected tight-binding Hamiltonians for an accurate quasiparticle description of topological insulators of the Bi_2Se_3 family, Phys. Rev. B 100 (2019) 155147, http://dx.doi.org/10.1103/PhysRevB.100.155147.

[22] K.W. Post, B.C. Chapler, L. He, X. Kou, K.L. Wang, D.N. Basov, Thickness-dependent bulk electronic properties in Bi_2Se_3 thin films revealed by infrared spectroscopy, Phys. Rev. B 88 (2013) 075121, http://dx.doi.org/10.1103/PhysRevB.88.075121.

[23] M. Orlita, B.A. Piot, G. Martinez, N.K.S. Kumar, C. Faugeras, M. Potemski, C. Michel, E.M. Hankiewicz, T. Brauner, Č. Drašar, S. Schreyeck, S. Grauer, K. Brunner, C. Gould, C. Brüne, L.W. Molenkamp, Magneto-optics of massive Dirac Fermions in bulk Bi_2Se_3, Phys. Rev. Lett. 114 (2015) 186401, http://dx.doi.org/10.1103/PhysRevLett.114.186401.

[24] G. Martinez, B.A. Piot, M. Hakl, M. Potemski, Y.S. Hor, A. Materna, S.G. Strzelecka, A. Hruban, O. Caha, J. Novák, A. Dubroka, Č. Drašar, M. Orlita, Determination of the energy band gap of Bi_2Se_3, Sci. Rep. 7 (2017) 6891, http://dx.doi.org/10.1038/s41598-017-07211-x.

[25] H. Köhler, A. Fabbicius, Galvanomagnetic properties of Bi_2Se_3 with free carrier densities below 5×10^{17} cm^{-3}, Phys Status Solidi B 71 (1975) 487–496, http://dx.doi.org/10.1002/pssb.2220710209.

[26] T. Kotani, M. van Schilfgaarde, S.V. Faleev, Quasiparticle self-consistent *GW* method: A basis for the independent-particle approximation, Phys. Rev. B 76 (2007) 165106, http://dx.doi.org/10.1103/PhysRevB.76.165106.

[27] T. Kotani, M. van Schilfgaarde, Fusion of the LAPW and LMTO methods: The augmented plane wave plus muffin-tin orbital method, Phys. Rev. B 81 (2010) 125117, http://dx.doi.org/10.1103/PhysRevB.81.125117.

[28] F. Matsui, S. Makita, H. Matsuda, T. Yano, E. Nakamura, K. Tanaka, S. Suga, S. Kera, Photoelectron momentum microscope at BL6U of UVSOR-III synchrotron, Japan. J. Appl. Phys. 59 (2020) 067001, http://dx.doi.org/10.35848/1347-4065/ab9184.

[29] D. Deguchi, K. Sato, H. Kino, T. Kotani, Accurate energy bands calculated by the hybrid quasiparticle self-consistent *GW* method implemented in the ecalj package, Japan. J. Appl. Phys. 55 (2016) 051201, http://dx.doi.org/10.7567/JJAP.55.051201.

[30] T. Kotani, ecalj package, URL https://github.com/tkotani/ecalj.

[31] C.P. Vicente, J.L. Tirado, K. Adouby, J.C. Jumas, A.A. Touré, G. Kra, X-ray diffraction and ^{119}Sn Mössbauer Spectroscopy Study of a New Phase in the Bi_2Se_3-SnSe System: $SnBi_4Se_7$, Inorg. Chem. 38 (1999) 2131–2135, http://dx.doi.org/10.1021/ic9812858.

[32] V.V. Atuchin, S.V. Borisov, T.A. Gavrilova, K.A. Kokh, N.V. Kuratieva, N.V. Pervukhina, Physical vapor transport growth and morphology of Bi_2Se_3 microcrystals, Particuology 26 (2016) 118–122, http://dx.doi.org/10.1016/j.partic.2015.10.003.

[33] O. Chiatti, C. Riha, D. Lawrenz, M. Busch, S. Dusari, J. Sánchez-Barriga, A. Mogilatenko, L.V. Yashina, S. Valencia, A.A. Ünal, O. Rader, S.F. Fischer, 2D layered transport properties from topological insulator Bi_2Se_3 single crystals and micro flakes, Sci. Rep. 6 (2016) 27483, http://dx.doi.org/10.1038/srep27483.

[34] L.A. Wray, S.Y. Xu, Y. Xia, Y.S. Hor, D. Qian, A.V. Fedorov, H. Lin, A. Bansil, R.J. Cava, M.Z. Hasan, Observation of topological order in a superconducting doped topological insulator, Nat. Phys. 6 (2010) 855–859, http://dx.doi.org/10.1038/nphys1762.

[35] R.C. Hatch, M. Bianchi, D. Guan, S. Bao, J. Mi, B.B. Iversen, L. Nilsson, L. Hornekær, P. Hofmann, Stability of the Bi_2Se_3 (111) topological state: Electron-phonon and electron-defect scattering, Phys. Rev. B 83 (2011) 241303, http://dx.doi.org/10.1103/PhysRevB.83.241303.

[36] See Supplementaly Material, URL https://doi.org/10.1016/j.vacuum.2024.113944.